PAPER

# Thermal transport in beta-gallium oxide thin-films using non-gray Boltzmann transport equation



IOP Publishing Journal of Physics: Condensed Matter
J. Phys.: Condens. Matter **34** (2022) 105603 (11pp) https://doi.org/10.1088/1361-648X/ac413e

# Thermal transport in beta-gallium oxide thin-films using non-gray Boltzmann transport equation

**Nitish Kumar, Matthew C Barry and Satish Kumar***

G.W. Woodruff School of Mechanical Engineering, Georgia Institute of Technology, Atlanta, United States of America

E-mail: satish.kumar@me.gatech.edu

Received 18 August 2021, revised 30 November 2021
Accepted for publication 8 December 2021
Published 24 December 2021

**Abstract**

Phonon transport in $\beta$-$Ga_2O_3$ thin films and metal-oxide field effect transistors (MESFETs) are investigated using non-gray Boltzmann transport equations (BTEs) to decipher the effect of ballistic-diffusive phonon transport. The effects of domain size, and energy dissipation to various phonon modes and subsequent phonon–phonon energy exchange on the thermal transport and temperature distribution is investigated using non-gray BTE. Our analysis deciphered that domain size plays a major role in thermal transport in $\beta$-$Ga_2O_3$ but energy dissipation to various phonon modes and subsequent phonon–phonon energy exchange does not affect the temperature field significantly. Phonon transport in $\beta$-$Ga_2O_3$ MESFETs on diamond substrate is investigated using coupled non-gray BTE and Fourier model. It is established that the ballistic effects need to be considered for devices with $\beta$-$Ga_2O_3$ layer thickness less than 1 $\mu$m. A non-gray phonon BTE model should be used near hotspot in the thin $\beta$-$Ga_2O_3$ layer as the Fourier model may not give accurate temperature distribution. The results from this work will help in understanding the mechanism of phonon transport in the $\beta$-$Ga_2O_3$ thin films and energy efficient design of its FETs.

Keywords: non-gray Boltzmann transport equation (BTE), $\beta$-$Ga_2O_3$, phonon transport, thermal transport, field effect transistors (FETs), wide bandgap materials

(Some figures may appear in colour only in the online journal)

## 1. Introduction

$\beta$-$Ga_2O_3$ is a promising candidate for next generation power and RF electronics [1–3]. The wider bandgap of $\beta$-$Ga_2O_3$ ($\sim$4.8 eV) helps it achieve significantly higher critical field strength compared to silicon and other widely used wide bandgap materials such as GaN and SiC. The superior electrical properties will enable $\beta$-$Ga_2O_3$ devices to operate at higher temperatures and voltages with higher efficiency [1–3]. It will help make $\beta$-$Ga_2O_3$ based electronic systems more powerful and efficient. The significant advantage of $\beta$-$Ga_2O_3$ in power and RF electronics is also evident through various figures of merit such as Baliga's figure of merit, Johnson's figure of merit etc [1, 4]. In addition, high-quality bulk crystals of $\beta$-$Ga_2O_3$ can be produced at low cost using melt growth techniques, which makes it very attractive for large-scale adaptation in many technologies [1]. The aforementioned advantages have significantly increased the interest of scientific community in $\beta$-$Ga_2O_3$.

In recent years, several $\beta$-$Ga_2O_3$-based FETs have been developed and a significant improvement in some of the parameters such as breakdown voltage, cut-off frequency, on/off ratio, contact resistance, maximum drain current, etc have been reported [1, 5–8]. However, efficient heat removal is still one of the biggest challenges for these devices due to low thermal conductivity. Green *et al* [9] have observed temperature induced catastrophic failure. The thermal conductivity of $\beta$-$Ga_2O_3$ varies between 10 and 29 W $mK^{-1}$ at room temperature, depending upon the crystal direction [10–12]. It is

* Author to whom any correspondence should be addressed.

 

significantly lower than that of GaN (150 W $mK^{-1}$) [13] and 4H–SiC (370 W $mK^{-1}$) [1]. The issue of efficient heat dissipation should become even more critical in the future devices with a further increase in power density. Since, electrical performance of the device is dependent upon the temperature, understanding of thermal characteristics of these devices is important in realizing the full potential of $\beta$-$Ga_2O_3$.

One of the most important aspects of accurate prediction of thermal behavior is appropriately considering the effect of size and dimensions of the devices. At smaller length scales, diffusive transport model may not predict the thermal transport accurately [14]. Heat transport in $\beta$-$Ga_2O_3$ is dominated by phonons [10, 11], which are quantized lattice vibrations. As the dimension of the system approaches the same order as of the phonon mean free path (mfp), ballistic transportation of the phonons also need to be considered. The heat transport is no longer purely diffusive, and Fourier's law may give erroneous results [15]. Therefore, a thermal transport model is needed, which can account for ballistic effects at smaller length scales and recover bulk diffusive behavior at larger length scales. Several types of models and techniques have been developed to study the thermal transport at smaller length scales such as atomistic modeling using molecular dynamics, mesoscale modeling using Boltzmann transport equation (BTE), etc [16, 17]. The semi-classical BTE is applicable when phonon wavelength is significantly smaller than characteristic lengths of the device. The wave nature of the phonons can be ignored, and phonons can be treated as semi-classical particles [18, 19]. The semi-classical phonon BTE has been widely used to describe the thermal transport in semiconductor devices [20–22]. This approach can also be used for $\beta$-$Ga_2O_3$ devices.

Phonon BTE is solved in both physical space of the geometry and wave-vector space of the phonons. The complex inter-phonon scattering terms need to be computed over the entire wave-vector space, which makes solving it very expensive and time-consuming for microscale geometries. A widely used approximation for the complex full scattering term is single mode relaxation time approximation (SMRTA), which allows implementation of phonon BTE for complex geometries with heat source and different boundary conditions. The main limitation of this approximation is that it cannot account for momentum conserving scattering (normal processes). However, these processes are only important at significantly lower temperatures than room temperatures. The effect of normal processes is negligible at room temperature and SMRTA agrees well with the experiments. Several studies have employed SMRTA successfully to study heat transport in the semiconductor devices including wide bandgap devices [18, 20, 21, 23]. Several other simplifications are also proposed such as gray BTE, and semi-gray BTE. Gray and semi-gray models incorporate single group velocity and relaxation time [24]. They can account for the ballistic effects and boundary scattering. However, they cannot predict temperature accurately because all the polarizations and full phonon dispersion are not considered. Narumanchi *et al* [25] compared gray and semi-gray BTE models against non-gray BTE model with full phonon dispersion and showed these models give erroneous results. Several other studies have solved BTE, where dispersion and polarization effects are considered [20, 26, 27].

However, non-gray BTE model with full phonon dispersion involves solving for all the phonon modes in each physical cell. It requires solving a large number of equations simultaneously and makes the non-gray BTE modeling computationally expensive. In the conventional solution approach, known as sequential method, a phonon mode is chosen and solved over entire physical domain before moving to the next phonon mode. However, this method suffers from slow convergence at low Knudsen numbers (Kn = phonon mfp/characteristic length) because of the increased amount of phonon scattering can tightly couple the discrete equations [18]. Loy *et al* [22] developed an alternative method, known as coupled ordinates method (COMET). In the COMET, the process is reversed, and all the phonon modes are solved in a cell before moving to the next cell. COMET is the better approach to solve the non-gray BTE for $\beta$-$Ga_2O_3$ devices, where most of the phonon modes have mfps smaller than the device characteristics lengths.

Non-gray BTE has been used to study thermal transport in GaN FETs, but it has not been used to study thermal transport in $\beta$-$Ga_2O_3$ FETs yet. For GaN FETs, it has been shown that Fourier's law may not be able to accurately predict the temperature distribution [20, 28]. In all the previous works, diffusive thermal transport models have been used to study thermal transport in $\beta$-$Ga_2O_3$ FETs [29–31]. Even though a few studies [12, 32] have employed non-gray BTE to predict phonon properties and bulk thermal conductivity, the effect of size on thermal transport in $\beta$-$Ga_2O_3$ films and FETs is not known. It is important to study thermal transport in $\beta$-$Ga_2O_3$ films and FETs using non-gray BTE and estimate the accuracy of Fourier model in predicting temperature for various device dimensions.

In this work, non-gray BTE is solved for $\beta$-$Ga_2O_3$ thin films and its FETs to investigate its thermal characteristics. First, the effect of film thickness on the $\beta$-$Ga_2O_3$ thermal conductivity is investigated at room temperature. It is shown that thermal conductivity increases sharply as the film thickness increases up to around 1 $\mu$m film thickness and then it asymptotically approaches the bulk thermal conductivity value. Next, the effect of domain size and mechanism of the energy dissipation to various phonon modes on the temperature distribution in the domain is studied. The difference in the hotspot temperatures predicted using Fourier's law and non-gray BTE are compared for three different domain sizes. We demonstrate that domain size plays an important role in thermal transport in $\beta$-$Ga_2O_3$ but energy dissipation to various phonon modes and subsequent phonon–phonon energy exchange does not affect the temperature field significantly. Finally, thermal transport in $\beta$-$Ga_2O_3$ metal-oxide field effect transistor (MESFET) integrated with a high thermal conductivity diamond substrate is studied. The ballistic-diffusive thermal transport and its dependence on the $\beta$-$Ga_2O_3$ layer thickness is explored. The error in the temperature prediction using Fourier's law in these devices is estimated for different thicknesses of $\beta$-$Ga_2O_3$ layer. The Fourier model may not give accurate temperature distribution and non-gray phonon BTE model should be used near hotspot in the $\beta$-$Ga_2O_3$ layers of thickness less than 1 $\mu$m. The

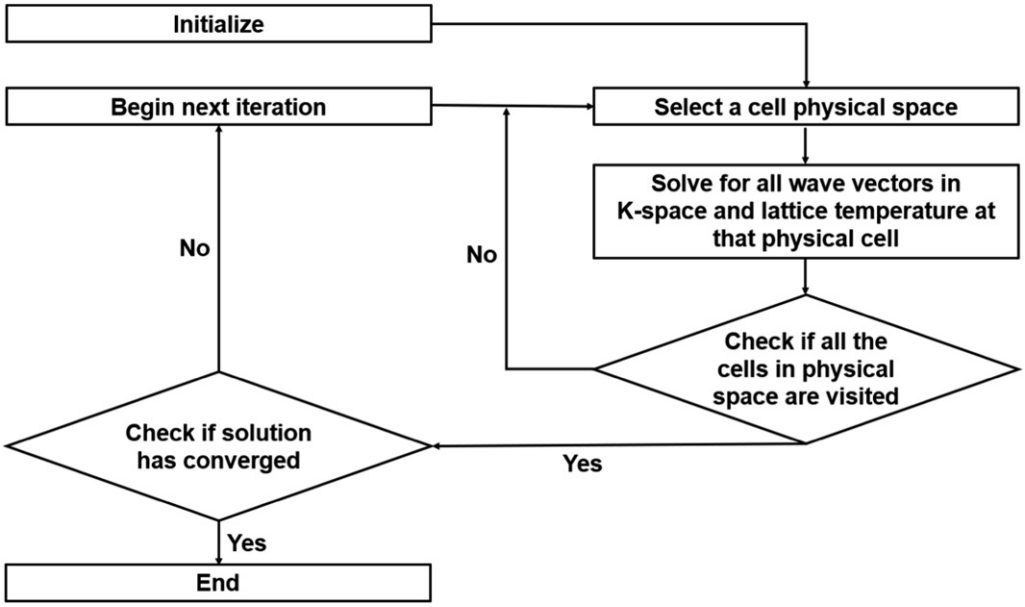


**Figure 1.** Flowchart of non-gray BTE simulations.

importance of solving non-gray phonon BTE model in $\beta$-$Ga_2O_3$ layer to predict accurate temperature profile in these devices is highlighted.

## 2. Methodology

### *2.1. Non-gray phonon BTE simulations*

The steady-state non-gray BTE of a phonon mode under single-mode relaxation time approximation (SMRTA) [19] is given by equation (1). It is discretized using finite volume method as shown in equation (2)

$$v \cdot \nabla e' = \frac{e^0 - e''}{\tau_{\text{eff}}} + S'''_{\text{vol}}. \tag{1}$$

Equation (1) is integrated over both physical and *k*-space control volumes. Then, divergence theorem is applied, and discretization is done to obtain equation (2)

$$\iint \left[ v \cdot \nabla e'' = \frac{e^0 - e''}{\tau_{\text{eff}}} + S'''_{\text{vol}} \right] \mathrm{d}V \, \mathrm{d}^3K.$$

$$\sum_{\text{f}} e''_{\text{f}} v \cdot \nabla A_{\text{f}} = \frac{e^0_{\text{c}} - e''_{\text{c}}}{\tau_{\text{eff}}} \Delta V + S_{\text{vol}} \tag{2}$$

$$e^0 = \hbar\omega = \frac{\hbar\omega}{\exp\left(\frac{\hbar\omega}{K_{\text{B}}T}\right) - 1} \tag{3}$$

As phonon scattering process is redistributive, integral of scattering term over entire *k*-space, including all polarizations, in a given cell should be zero. It represents energy conservation in each physical cell [22] and given by equation (4)

$$\int \frac{e^0 - e''}{\tau_{\text{eff}}} \mathrm{d}^3K = 0. \tag{4}$$

Equation (5) is obtained after discretization. It can be solved for a lattice temperature in a physical cell to satisfy energy conservation

$$\sum \frac{e^0_{\text{c}}}{\tau_{\text{eff}}} \Delta^3 K - \sum \frac{e''_{\text{c}}}{\tau_{\text{eff}}} \Delta^3 K = 0. \tag{5}$$

Here, subscript c and f denote that value is calculated at centroid and face of a cell, respectively. The $e''$ is the energy density of the phonon mode, $v$ is the phonon group velocity, $\nabla A$ is the area vector associated with a face in the physical domain, and $e^0$ is the equilibrium energy density, $\tau_{\text{eff}}$ is the effective phonon relaxation time, which accounts for contribution from different scattering mechanisms, $\omega$ is the phonon frequency, $\Delta V$ represents the volume of a cell in physical space, $S'''_{\text{vol}}$ is external volumetric heat source and $S_{\text{vol}}$is the external heat source in a physical cell $\Delta V$, $\hbar$ is reduced Planck's constant, $K_{\text{B}}$ is Boltzmann constant and $N$ is the equilibrium Bose–Einstein distribution for a phonon mode of frequency $\omega$, and polarization $p$ at temperature $T$. Direct coupling of all these BTEs is extremely expensive to solve. RTA is used to simplify the scattering term on the right-hand side of the BTE. Two different types of boundary conditions are considered in this work: (1) constant temperature and (2) specular reflection (adiabatic). The details of implementation of these boundary conditions are available in [22, 33]. In the current study, the BTE will be solved iteratively using COMET. Then, all the phonon modes are directly solved together in a cell before moving to the next cell in physical space. This process is repeated until convergence is achieved. This method is parallelized such that physical mesh is divided into sub-meshes, which are solved by different processors to reduce calculation time. A flowchart of the COMET algorithm is presented in figure 1. The additional details on the solution of BTE using COMET algorithm are available in [22, 33].

The parameters such as, $v$ and $\tau_{\text{eff}}$ are different for different phonon modes. The phonon properties needed for non-gray BTE such as $\tau_{\text{eff}}$, $v$ and $\omega$ for $\beta$-$Ga_2O_3$, are obtained from density function theory (DFT) following the approach used in

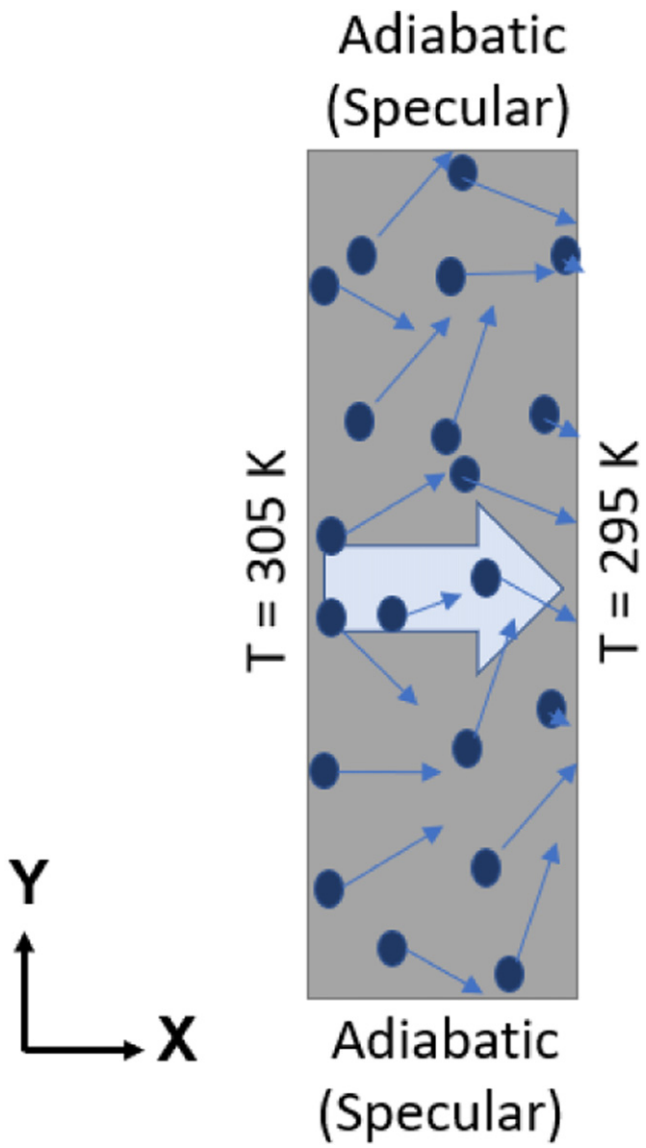


**Figure 2.** A schematic of thin film with the applied boundary conditions.

[12, 32]. Density functional theory (DFT) calculations are performed using the Vienna *ab initio* simulation package [34, 35]. A plane-wave basis set and the projector augmented-wave method [36, 37] are used with the Perdew–Burke–Ernzerhof exchange–correlation functional [38]. All DFT computations are performed using a plane-wave basis cutoff energy of 520 eV and a convergence criterion for the energy and forces of $10^{-9}$ eV and $10^{-6}$ eV $Å^{-1}$, respectively. The ten-atom primitive cell structure is optimized using a $16 \times 16 \times 8$ grid of *k*-points. The second-order harmonic and third-order anharmonic interatomic force constants (IFCs) are both calculated via the finite displacement method [39] using the $3 \times 3 \times 3$ supercell with a $2 \times 2 \times 2$ grid of *k*-points. The finite displacement distance is 0.01 Å and a 4th nearest neighbor cutoff is used for computing the third order IFCs. The phonon properties are computed using Fermi's golden rule [40] with the iterative solution to the BTE [41–43]. A $9 \times 7 \times 5$ mesh is used for sampling the Brillouin zone. The dielectric tensor and Born effective charges are calculated from density functional perturbation theory and included in the BTE calculations to account for the longitudinal and transverse optical phonon splitting at the $\Gamma$ point.

### 2.2. Multiscale electrothermal simulations

The size of $\beta$-$Ga_2O_3$ MESFETs can be significantly larger as substrate thickness are typically of the order of a few hundreds of microns. Therefore, it is impractical and computationally very expensive to solve the phonon BTE in the entire MESFET. The Joule heating occurs only in the semiconducting $\beta$-$Ga_2O_3$ layer in the MESFETs. The thermal transport becomes diffusive away from the heat source. Therefore, the BTE needs to be solved only in the semiconducting $\beta$-$Ga_2O_3$ layer, where ballistic-diffusive effects are significant. Fourier's law should be applicable away from the heat source in the substrate, where thermal transport is diffusive. The two models are coupled together to predict temperature distribution in the entire device.

## 3. Results and discussion

### 3.1. Effect of film thickness on thermal conductivity

The non-gray phonon BTE is employed to estimate the effect of film thickness on thermal conductivity of $\beta$-$Ga_2O_3$. A schematic of the $\beta$-$Ga_2O_3$ film is shown in figure 2. The thermal conductivity is measured at room temperature. Therefore, 305 K and 295 K are applied at left and right edge of the film. The top and the bottom edge are insulated, where the specular reflection boundary condition is applied to simulate infinite thickness in vertical (*y*-axis) direction. The thermal conductivity is computed in two crystal direction—(100) and (010). These two directions are perpendicular to each other in the crystal. Even though $\beta$-$Ga_2O_3$ has anisotropic thermal conductivity, it can be approximated to be bi-directional because conductivity in all directions in the plane perpendicular to (010) are very close [10]. Therefore, (100) direction is considered to be representative of all these directions. The conductivity in each crystal direction is calculated by aligning that direction along *x*-axis and the other direction along *y*-axis in the simulations.

Figure 3 shows thermal conductivity of the $\beta$-$Ga_2O_3$ thin films as a function of film thickness. It can be observed that thermal conductivity increases as the film thickness increases and asymptotically approaches the bulk conductivity. The bulk thermal conductivity predicted in this study is in good agreement with the experimentally measured bulk values in both the crystal directions as shown in table 1. Thin film conductivity is less than bulk conductivity because some of the phonon modes with mfps larger than film thickness have their contribution to conductivity restricted. In other words, the mfps of these modes is reduced to film thickness and, therefore, thermal conductivity is reduced. The largest phonon mfp for $\beta$-$Ga_2O_3$ is around 0.5 $\mu$m. The initial sharp change in thermal conductivity up to around 1 $\mu$m is due to significant ballistic transport in the films with thickness less than 1 $\mu$m. Beyond 1 $\mu$m thickness, thermal conductivity gradually approaches the bulk value.

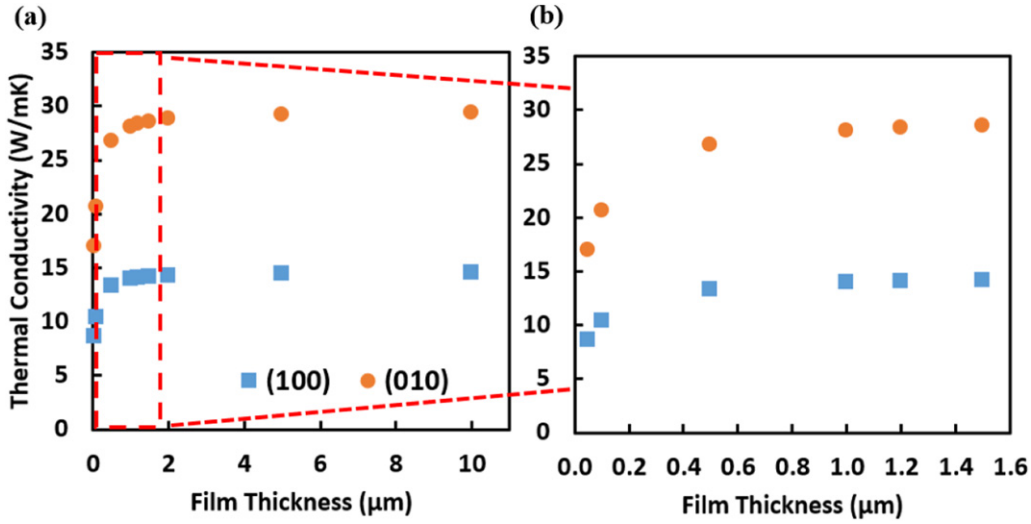


**Figure 3.** (a) Effect of film thickness on $\beta$-$Ga_2O_3$ thermal conductivity. (b) A close-up view of figure 3(a).

**Table 1.** Comparison of bulk thermal conductivity predicted in this study with the measured values in the literature.

| Crystal direction | Experiments (W $mK^{-1}$) | This study (W $mK^{-1}$) |
|---|---|---|
| 100 | $10.9 \pm 1$ [10]; $13 \pm 1$ [47] | 14.5 |
| 010 | $27 \pm 2$ [10]; 29.21 [11] | 29.2 |

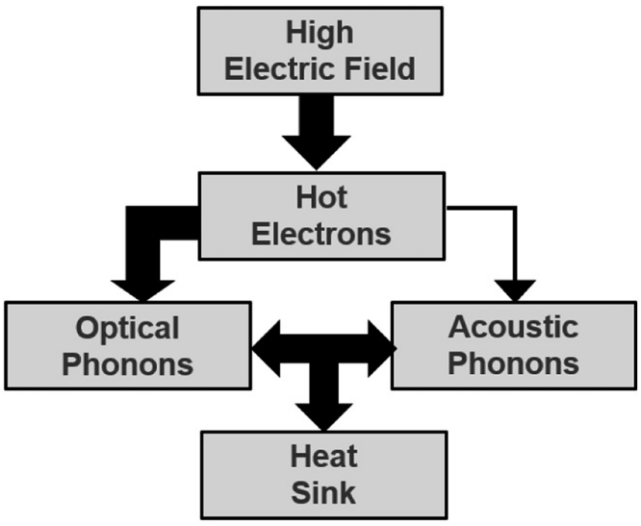


**Figure 4.** Energy exchange pathway for semiconductors during Joule heating.

### 3.2. *Temperature distribution in $\beta$-$Ga_2O_3$ with Joule heating*

Next, we investigate the effect of $\beta$-$Ga_2O_3$ domain size and energy dissipation to various phonon modes on thermal transport and temperature distribution using non-gray BTE model. We compared the temperature distribution obtained from the Fourier's law and non-gray BTE simulations. In semiconductor devices, high electric field leads to hot carriers (hole or electrons) that have attained very high kinetic energy. These hot carriers interact with lattice and transfer energy to the

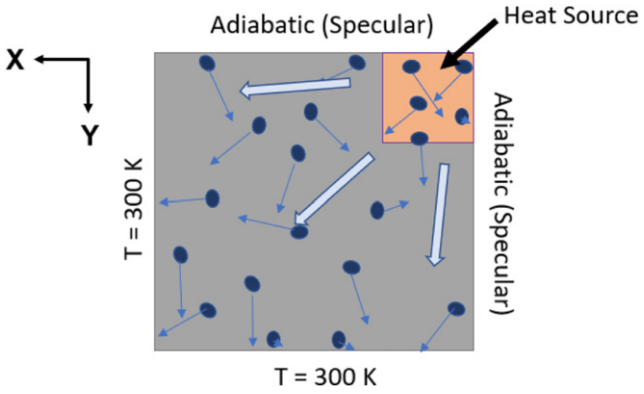


**Figure 5.** A schematic of $\beta$-$Ga_2O_3$ domain, heat source and the applied boundary conditions.

vibrational modes, i.e., phonons. Most of the energy is transferred to the optical phonons during these interactions [28, 44], which may lead to non-equilibrium in the temperatures of different phonon modes near heat source, where electron–phonon interactions take place. These optical phonons then interact with acoustic phonons and the energy is conducted to the heat sink primarily by these phonons. Figure 4 depicts a typical energy exchange pathway in semiconductor devices in case of Joule heating. In addition to complex phonon interactions, size of the domain can also affect the thermal transport. We have already observed in the last section that thermal conductivity of $\beta$-$Ga_2O_3$ is significantly affected by the film thickness.

A $\beta$-$Ga_2O_3$ domain with a heat source and applied boundary conditions is chosen as shown in figure 5. The top and right edge are insulated where specular reflection boundary condition is applied. Isothermal boundary condition is applied at the bottom and left edge and temperature is set at 300 K. A heat source of size 0.1 $\mu$m $\times$ 0.1 $\mu$m was chosen. In $\beta$-$Ga_2O_3$, the electron–phonon scattering is dominated by high frequency optical phonons. Optical phonons near $\Gamma$-point in Brillouin zone and with frequency of 235 $cm^{-1}$ (29 meV) or greater are determined to be strongly coupled with electrons [45]. Since,

**Table 2.** Comparison of peak temperatures depending upon model employed. The error is calculated with respect to NG BTE-20 model.

| Model | Description | Peak temperature (K) | % Error |
|---|---|---|---|
| NG BTE-30 | Heat source is applied to all 30 modes equally | 587.0 | 0.9 |
| NG BTE-20 | Heat source is applied to top 20 modes equally | 589.7 | — |
| NG BTE-1 | Heat source is applied to 30th mode only | 589.6 | <0.01 |
| Fourier-bulk | Conductivity is chosen from 5 $\mu$m film | 578.2 | 4.0 |
| Fourier-1 | Conductivity is chosen from 1 $\mu$m film | 587.2 | 0.8 |

**Table 3.** Comparison of peak temperatures predicted using Fourier's law and non-gray BTE for different domain size.

| Domain size | Peak temperature (K) using Fourier-bulk | Peak temperature (K) using NG BTE-20 | % Error in peak temperature |
|---|---|---|---|
| 1.1 $\mu$m × 1.1 $\mu$m | 578.2 | 589.7 | 4.0 |
| 0.6 $\mu$m × 0.6 $\mu$m | 506.4 | 522.4 | 7.2 |
| 0.2 $\mu$m × 0.2 $\mu$m | 392.7 | 415.7 | 19.8 |

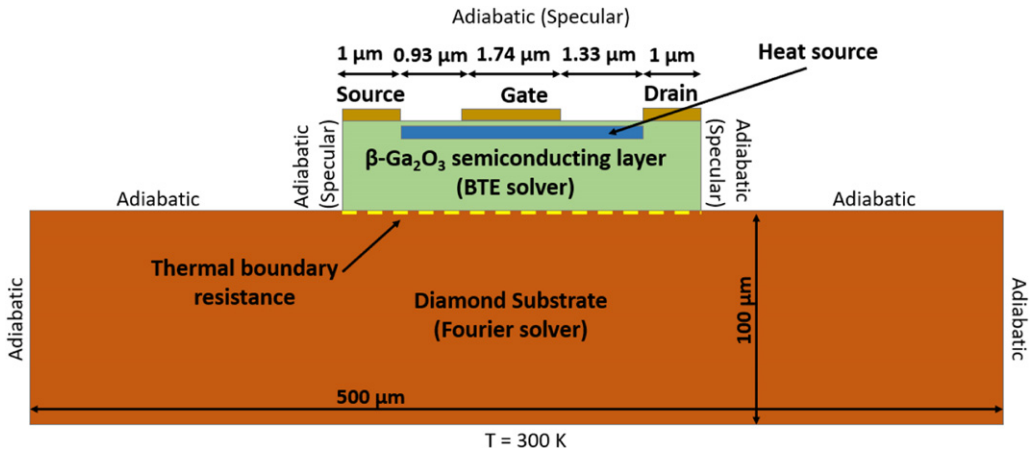


**Figure 6.** Schematic of a $\beta$-$Ga_2O_3$ FET on diamond substrate.

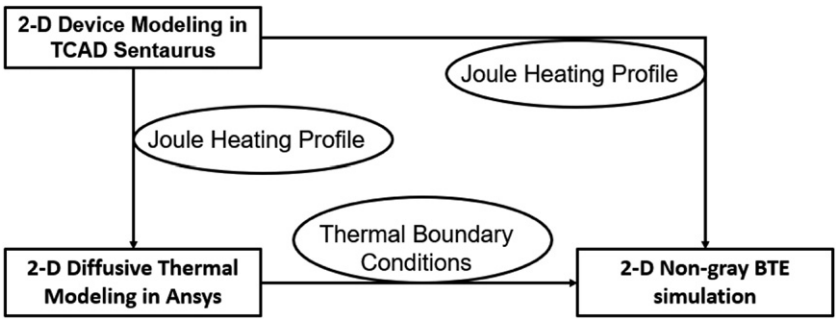


**Figure 7.** A flowchart of the procedure of multiscale modeling. Non-gray BTE model is used for $\beta$-$Ga_2O_3$ layer and Fourier model is used for the diamond substrate.

the exact distribution of hot electron energy to all the optical phonon modes is not available in the literature. Therefore, in the first case (referred as NG BTE-20), Joule heat is equally distributed in the top 20 phonon modes with largest frequency out of total 30 modes, at the nearest $k$-points to $\Gamma$-point in each direction. These 20 modes are all optical modes and have frequency greater than or equal to $\sim$235 cm$^{-1}$. In second case (referred as NG BTE-1), we applied heat source to the mode with highest frequency near $\Gamma$-point. In third case, (referred as NG BTE-30), we applied heat source to all the 30 modes equally near $\Gamma$-point. Initially, a non-gray BTE domain of size 1.1 $\mu$m × 1.1 $\mu$m was chosen as size effects are expected to be small. Table 2 shows comparison between peak temperature predicted using Fourier's law and non-gray BTE models. First, if we compare the three cases of non-gray BTE model, where heat source is applied to different modes, there is negligible difference in the peak temperature predicted by them. Especially, when heat source is applied only to optical modes

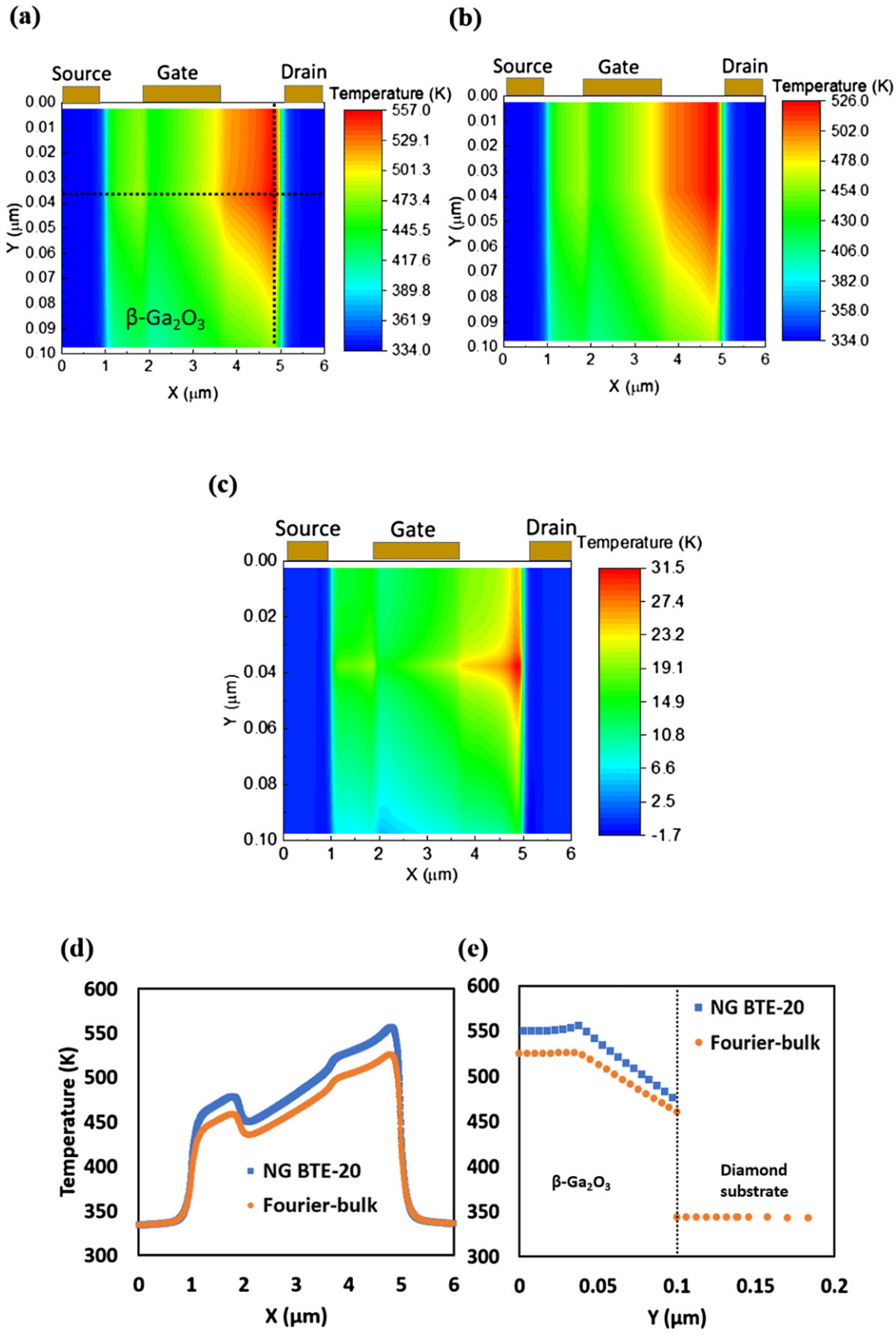


**Figure 8.** Temperature field predicted (a) using non-gray BTE (NG BTE-20) and Fourier coupled model, and (b) using Fourier model only. (c) Contour plot of the temperature difference predicted from the NG BTE-20 and Fourier model ($T_{\mathrm{BTE}} - T_{\mathrm{FOURIER}}$). (d) Comparison of temperature profiles predicted using non-gray BTE (NG BTE-20) and Fourier model along the horizontal dotted line ($Y \sim 0.0375$ $\mu$m) and (e) the vertical dotted line ($X \sim 4.81$ $\mu$m).

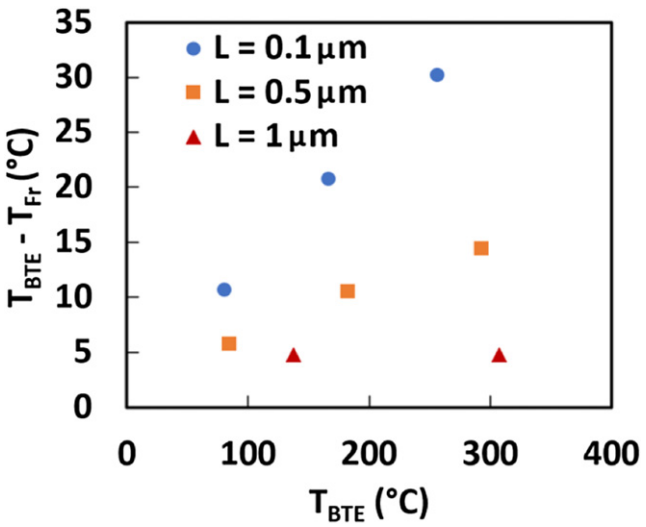


**Figure 9.** Error in the Fourier predicted peak temperature as a function of non-gray BTE predicted peak temperature.

(NG BTE-20 and NG BTE-1), the temperatures are same. However, when the heat source is applied to all the modes including acoustic modes (NG BTE-30), there is a drop of 2 K in peak temperature compared to NG BTE-20 and NG BTE-1. This trend was expected because acoustic modes have longer mfps than optical modes, but the effect is less as most of the modes are optical modes (∼27 out of 30 modes). From these three cases, we can conclude that the distribution of energy transfer to various phonon modes and phonon–phonon energy exchange do not play any significant role in the temperature prediction.

Next, we calculated peak temperature using Fourier's law with two different thermal conductivities. In the first case (referred as Fourier-bulk), we use thermal conductivity corresponding to 5 $\mu$m film, where bulk conductivity has been recovered and there are negligible ballistic transport effects. In second case (referred as Fourier-1), we use thermal conductivity corresponding to 1 $\mu$m film. We can observe from table 2 that there is difference between peak temperatures predicted using Fourier-bulk and Fourier-1 due to ballistic thermal transport in Fourier-1 but it is small (<4%). However, the thermal transport in domains larger than 1 $\mu$m is primarily diffusive. In addition, if we compare the peak temperature predicted using Fourier's law models and non-gray models, we observe that the difference is not significant. Therefore, ballistic effects due to the size of the domain, when domain size is around 1 $\mu$m or larger, are not important in prediction of temperature field. Retrospectively, it could have been also anticipated from thin film thickness versus conductivity trend of figure 3 as conductivity nearly attains bulk conductivity value for film thickness of 1 $\mu$m or larger, given that phonon–phonon non-equilibrium effects do not affect the peak temperature.

However, as the domain size is reduced below 1 $\mu$m, the ballistic effects starts playing bigger role in the thermal transport and Fourier's law will not give accurate results. Three different domain sizes—0.2 $\mu$m × 0.2 $\mu$m, 0.6 $\mu$m × 0.6 $\mu$m and 1.1 $\mu$m × 1.1 µm—of $\beta$-$Ga_2O_3$ were chosen. As the domain size is decreased from 1.1 $\mu$m × 1.1 $\mu$m to 0.6 $\mu$m × 0.6 $\mu$m and then to 0.2 $\mu$m × 0.2 $\mu$m, we observed that the Fourier's law starts underpredicting the peak temperature as ballistic transport of phonons becomes important. Fourier-bulk does not account for the size of the domain because bulk thermal conductivity is used for all three domains with different sizes. On the other hand, non-gray BTE model accounts for size effects. The phonons with mfp larger than domain size travel ballistically and scatter at the boundary. Thus, the effective thermal conductivity of the domain is reduced in non-gray BTE model, as discussed in section 3.1, and peak temperature predicted by non-gray BTE model is higher than that by Fourier model. Table 3 compares the peak temperatures predicted using Fourier-bulk and NG BTE-20. We can observe that % error in temperature prediction for the three domains—1.1 $\mu$m × 1.1 $\mu$m, 0.6 $\mu$m × 0.6 $\mu$m and 0.2 $\mu$m × 0.2 $\mu$m are 4.0%, 7.2% and 19.8%, respectively. The error is increasing as the domain size decreases, which implies that ballistic effects become more important as the domain size decreases.

## 4. Multiscale modeling of $\beta$-$Ga_2O_3$ FETs

Finally, we investigate whether phonon ballistic transport play a role in heat dissipation in $\beta$-$Ga_2O_3$ devices. Diamond is a promising candidate to be used as a substrate for $\beta$-$Ga_2O_3$ devices due to its high thermal conductivity. However, $\beta$-$Ga_2O_3$ and diamond heterointerface can be source of phonon scattering, which can affect the efficient heat dissipation from the hotspot. A $\beta$-$Ga_2O_3$ device on a high conductivity diamond substrate is studied using a coupled BTE-Fourier model. We investigate the effect of thickness of semiconducting $\beta$-$Ga_2O_3$ layer on ballistic diffusive transport near the hotspot in the device.

A typical $\beta$-$Ga_2O_3$-on-diamond device structure is considered in this study. A schematic of the device is shown in figure 6, where all the relevant dimensions are shown. A silicon delta-doping layer acts as a channel and most of the Joule heating occurs in this channel when the device is on. Electrothermal device modeling was performed using TCAD Sentaurus to obtain the Joule heat generation profile of the device at $V_{ds} = 10$ V, $V_{gs} = 2$ V and power $\sim 2$ W mm$^{-1}$ as described in [29, 30]. This profile is given as input in non-gray BTE and Fourier model simulations. The size of the device is large, so solving non-gray BTE model in the entire domain is impracticable. In addition, given the size of substrate, the thermal transport will be diffusive in it. Therefore, Fourier's law can be used in the substrate to study thermal transport. On the other hand, the $\beta$-$Ga_2O_3$ layer thickness is significantly smaller than the substrate, so ballistic transport may occur. Therefore, non-gray BTE model is used in the $\beta$-$Ga_2O_3$ layer. The diffuse scattering is assumed at the $\beta$-$Ga_2O_3$-diamond interface and the thermal boundary resistance is considered to be $5.59 \times 10^{-9}$ m$^2$ W K$^{-1}$ [46]. Specular reflection boundary condition is assumed at the remaining surfaces of the $\beta$-$Ga_2O_3$ layer (see BTE domain in figure 6). The bottom of the substrate is set to 300 K and rest of the surfaces are considered to be adiabatic in Fourier model. The thermal conductivity of the

**Table 4.** Comparison of peak temperatures predicted using Fourier-bulk model in Ansys and coupled BTE-Fourier model for different device thickness.

| Device thickness (μm) | Power (W mm$^{-1}$) | Peak temperature (K) using NG BTE-20 and Fourier coupled | Peak temperature (K) using Fourier model only | % Error in peak temperature |
|---|---|---|---|---|
| 0.1 | 20.4 | 381 | 370.3 | 13.2 |
| 0.1 | 40.8 | 466.6 | 445.8 | 12.4 |
| 0.1 | 61.2 | 556.2 | 526.0 | 11.8 |
| 0.5 | 10.2 | 384.8 | 379.0 | 6.8 |
| 0.5 | 20.4 | 482.4 | 471.8 | 5.8 |
| 0.5 | 30.6 | 592.5 | 578.1 | 4.9 |
| 1 | 10.2 | 437.4 | 432.7 | 3.5 |
| 1 | 20.4 | 607.6 | 602.8 | 1.6 |

diamond is considered to be 2169 W mK$^{-1}$ [46] for the Fourier model.

Figure 7 presents a flowchart of the procedure to run non-gray BTE in $\beta$-$Ga_2O_3$ layer and Fourier model in diamond substrate. First, Fourier model is run in the entire device with Joule heat generation profile obtained from TCAD Sentaurus as an input. The thickness and temperature dependence thermal conductivity of $\beta$-$Ga_2O_3$ layer is considered as well in this simulation. It provides the temperature distribution in the substrate and at the $\beta$-$Ga_2O_3$-diamond interface. The interface temperature is applied as a boundary condition and Joule heat generation profile obtained from TCAD Sentaurus as an input to the non-gray BTE simulations (NG BTE-20 case from section 3.2) to obtain the temperature field in $\beta$-$Ga_2O_3$ layer. In addition, the Fourier model is also solved in the entire domain with temperature dependent bulk thermal conductivity of $\beta$-$Ga_2O_3$ to compare the predictions with the BTE model (Fourier-bulk case from section 3.2). This model does not account for $\beta$-$Ga_2O_3$ layer thickness effects and is purely diffusive.

Three different device structures with thicknesses of $\beta$-$Ga_2O_3$ layer—0.1 $\mu$m (device-1), 0.5 $\mu$m (device-2) and 1 $\mu$m (device-3), are studied. These devices are operated at various power settings, which are applied by scaling the TCAD Sentaurus Joule heat profile obtained at $V_{ds} = 10$ V and $V_{gs} = 2$ V to match the desired power setting. Figures 8(a)–(e) shows comparison between the temperature field obtained using non-gray BTE and Fourier model for device-1 at power dissipation = 61.2 W mm$^{-1}$. Figures 8(a) and (b) shows the temperature profiles predicted using non-gray BTE and Fourier model, respectively. We can observe that location of peak temperature (hotspot) is predicted in the same region by both models. The peak temperature is located, toward the drain-side gate edge, where Joule heating density is high. The high Joule heating near the drain-side gate edge has also been shown in the previous studies [29, 30]. Even though temperature profiles predicted using the two models are qualitatively similar, there is quantitative difference between the two profiles. The Fourier model underpredicts the temperature as it cannot account for ballistic phonon transport. Figure 8(c) shows the spatial variation in the difference in temperature predicted by non-gray BTE and Fourier models. The largest error in the temperature is near the hotspot. In figures 8(d) and (e), the non-gray BTE and Fourier temperature are plotted along $x$ and $y$ axes, respectively, on a line passing through the hotspot. In figure 8(d), temperature profiles follow Joule heat profile on the $x$-axis line. As shown in figure 8(e), the temperature plotted along the vertical line passing through hot spot remains constant up to 45 nm from top ($y \sim 0$) and then it decreases linearly till the $Ga_2O_3$-diamond interface. This is because heat source is located between $35 \leqslant y \leqslant 45$ nm and the top surface is adiabatic. The Joule heat dissipates through the interface into the substrate, and there is a temperature drop at the interface due to thermal boundary resistance. The temperature varies linearly along $y$-axis line in the diamond substrate as well, but the slope is significantly lower compared to the $Ga_2O_3$ layer because the conductivity of the diamond is significantly higher than the $Ga_2O_3$.

Figure 9 shows error in the Fourier predicted peak temperature as a function of non-gray BTE predicted peak temperature for different film thicknesses. Table 4 compares the peak temperature obtained using non-gray BTE and Fourier coupled model against Fourier model for different power settings and device structures with different $\beta$-$Ga_2O_3$ layer thickness. It is evident from table 4 that % error in peak temperature predicted using Fourier's law increases as the layer thickness decreases. For example, at power = 20.4 W mm$^{-1}$, the % error in peak temperatures predicted by Fourier model are 13.2%, 5.8% and 1.6% for 0.1 $\mu$m, 0.5 $\mu$m and 1 $\mu$m thick $\beta$-$Ga_2O_3$ layers, respectively. Because Fourier model does not consider the ballistic phonon transport effects, these effects become more prominent as the layer thickness decreases as we discussed in section 3.1. For layer thickness around 1 $\mu$m, the Fourier model can predict the temperature field with reasonable accuracy. It implies the ballistic transport is no longer significant and diffusive transport dominates for film thickness around 1 $\mu$m and greater. However, for a given layer thickness, the % error in the peak temperature decreases as power increases. For a layer thickness of 0.1 $\mu$m, % errors are 13.2%, 12.4% and 11.8% for powers 20.4 W mm$^{-1}$, 40.8 W mm$^{-1}$ and 61.2 W mm$^{-1}$, respectively. This slight decrease can be attributed to decrease in the mfps of phonons as temperature increases with increase in power. Since, mfp is product of phonon velocity and relaxation time, as temperature increases the relaxation time decreases due to increased scattering, which leads to decrease in mfp. For a given domain size, as the mfps decrease, the ballistic transport becomes less significant and diffusive transport becomes more important.

Therefore, the % error in temperatures predicted by Fourier model decreases as power increases for a given domain.

## 5. Conclusion

Non-gray BTE is used to study phonon transport in $\beta$-$Ga_2O_3$ thin films and MESFETs. 1D thermal transport in $\beta$-$Ga_2O_3$ thin films is studied and the dependence of the $\beta$-$Ga_2O_3$ thermal conductivity on the film thickness is determined at room temperature. The thickness dependence of the thermal conductivity in thin films is attributed to the ballistic phonon transport. As the film thickness increases from 50 nm to 10 $\mu$m, the thermal conductivity also increases in both crystal directions—(100) and (010), and gradually approaches the bulk thermal conductivity value as film thickness increases beyond 1 $\mu$m. Thermal transport in a 2D domain of the $\beta$-$Ga_2O_3$ with a heat source is studied using non-gray BTE. The effect of domain size and, the energy distribution to various phonon modes and subsequent phonon–phonon scattering (energy exchange) on thermal transport and temperature distribution is studied. The peak temperatures predicted using a Fourier model and non-gray BTE models where heat source is applied in different phonon modes are compared for different domain sizes. It is observed that the distribution of energy transfer to different optical phonon modes does not lead to any significant error in the temperature prediction. However, Fourier's law does not account for ballistic transport, so for domain with characteristics length smaller than 1 $\mu$m, Fourier's law may not accurately predict the temperature distribution. Finally, thermal transport in $\beta$-$Ga_2O_3$-on-diamond MESFETs at various power dissipation settings is studied using coupled non-gray BTE and Fourier model. The Fourier model alone cannot predict the temperature distribution accurately when the thickness of $\beta$-$Ga_2O_3$ layer is less than 1 $\mu$m as the thermal transport will be ballistic-diffusive in $\beta$-$Ga_2O_3$ layer. Therefore, non-gray phonon BTE should be solved in the thin $\beta$-$Ga_2O_3$ region of the device for accurate temperature predictions.

## Data availability statement

The data that support the findings of this study are available upon reasonable request from the authors.

## References


[1] Pearton S J, Yang J, Cary P H, Ren F, Kim J, Tadjer M J and Mastro M A 2018 A review of $Ga_2O_3$ materials, processing, and devices *Appl. Phys. Rev.* **5** 011301

[2] Higashiwaki M and Jessen G H 2018 Guest editorial: the dawn of gallium oxide microelectronics *Appl. Phys. Lett.* **112** 060401

[3] Higashiwaki M, Sasaki K, Murakami H, Kumagai Y, Koukitu A, Kuramata A, Masui T and Yamakoshi S 2016 Recent progress in $Ga_2O_3$ power devices *Semicond. Sci. Technol.* **31** 034001

[4] Jessen G *et al* 2017 Toward realization of $Ga_2O_3$ for power electronics applications *2017 75th Annual Device Research Conf. (DRC)*

[5] Xia Z *et al* 2019 $\beta$-$Ga_2O_3$ delta-doped field-effect transistors with current gain cutoff frequency of 27 GHz *IEEE Electron Device Lett.* **40** 1052–5

[6] Zhou H, Maize K, Qiu G, Shakouri A and Ye P D 2017 $\beta$-$Ga_2O_3$ on insulator field-effect transistors with drain currents exceeding 1.5 A $mm^{-1}$ and their self -heating effect *Appl. Phys. Lett.* **111** 092102

[7] Wong M H, Sasaki K, Kuramata A, Yamakoshi S and Higashiwaki M 2016 Field-plated $Ga_2O_3$ MOSFETs with a breakdown voltage of over 750 V *IEEE Electron Device Lett.* **37** 212–5

[8] Mun J K, Cho K, Chang W, Jung H-W and Do J 2019 2.32 kV breakdown voltage lateral $\beta$-$Ga_2O_3$ MOSFETs with source-connected field plate *ECS J. Solid State Sci. Technol.* **8** Q3079

[9] Green A J *et al* 2017 $\beta$-$Ga_2O_3$ MOSFETs for radio frequency operation *IEEE Electron Device Lett.* **38** 790–3

[10] Guo Z *et al* 2015 Anisotropic thermal conductivity in single crystal $\beta$-gallium oxide *Appl. Phys. Lett.* **106** 111909

[11] Slomski M, Blumenschein N, Paskov P P, Muth J F and Paskova T 2017 Anisotropic thermal conductivity of $\beta$-$Ga_2O_3$ at elevated temperatures: effect of Sn and Fe dopants *J. Appl. Phys.* **121** 235104

[12] Yan Z and Kumar S 2018 Phonon mode contributions to thermal conductivity of pristine and defective $\beta$-$Ga_2O_3$ *Phys. Chem. Chem. Phys.* **20** 29236–42

[13] Luo C-Y, Marchand H, Clarke D R and DenBaars S P 1999 Thermal conductivity of lateral epitaxial overgrown GaN films *Appl. Phys. Lett.* **75** 4151–3

[14] Chen G 2005 *Nanoscale Energy Transport and Conversion: A Parallel Treatment of Electrons, Molecules, Phonons, and Photons* (Oxford: Oxford University Press)

[15] Majumdar A 1993 Microscale heat conduction in dielectric thin films *J. Heat Transfer* **115** 7–16

[16] Barry M C, Wise K E, Kalidindi S R and Kumar S 2020 Voxelized atomic structure potentials: predicting atomic forces with the accuracy of quantum mechanics using convolutional neural networks *J. Phys. Chem. Lett.* **11** 9093–9

[17] Barry M C, Yan Z, Yoon M, Kalidindi S R and Kumar S 2018 Phonon transport properties of two-dimensional electride $Ca_2N$—a first-principles study *Appl. Phys. Lett.* **113** 131902

[18] Loy J M 2010 An acceleration technique for the solution of the phonon Boltzmann transport equation *MS thesis* Purdue University

[19] Hess K 1988 Boltzmann transport equation *The Physics of Submicron Semiconductor Devices* (Berlin: Springer) pp 33–43

[20] Vallabhaneni A K, Chen L, Gupta M P and Kumar S 2017 Solving nongray Boltzmann transport equation in gallium nitride *J. Heat Transfer* **139** 102701

[21] Vallabhaneni A K, Loy J, Singh D, Ruan X and Murthy J Y 2013 A study of spatially-resolved non-equilibrium in laser-irradiated graphene using Boltzmann transport equation *ASME Int. Mechanical Engineering Congress and Exposition* (American Society of Mechanical Engineers)

[22] Loy J M, Mathur S R and Murthy J Y 2015 A coupled ordinates method for convergence acceleration of the phonon Boltzmann transport equation *J. Heat Transfer* **137** 012402

[23] Donmezer F N, Singh D, James W, Christensen A, Graham S and Murthy J Y 2011 Lattice Boltzmann and discrete ordinates methods for phonon transport modeling: a comparative study *ASME 2011 Int. Mechanical Engineering Congress and Exposition*

[24] Murthy J Y, Narumanchi S V J, Pascual-Gutierrez J A, Wang T, Ni C and Mathur S R 2005 Review of multiscale simulation in submicron heat transfer *Int. J. Multiscale Comput. Eng.* **3** 5–32

[25] Narumanchi S V J, Murthy J Y and Amon C H 2005 Comparison of different phonon transport models for predicting heat

conduction in silicon-on-insulator transistors *J. Heat Transfer* **127** 713–23
[26] Ali S A and Mazumder S 2015 Phonon heat conduction in multidimensional heterostructures: predictions using the Boltzmann transport equation *J. Heat Transfer* **137** 102401
[27] Ali S A, Kollu G, Mazumder S, Sadayappan P and Mittal A 2014 Large-scale parallel computation of the phonon Boltzmann transport equation *Int. J. Therm. Sci.* **86** 341–51
[28] Donmezer N, Islam M, Yoder P D and Graham S 2015 The impact of nongray thermal transport on the temperature of AlGaN/GaN HFETs *IEEE Trans. Electron Devices* **62** 2437–44
[29] Kumar N, Joishi C, Xia Z, Rajan S and Kumar S 2019 Electrothermal characteristics of delta-doped $\beta$-$Ga_2O_3$ metal–semiconductor field-effect transistors *IEEE Trans. Electron Devices* **66** 5360–6
[30] Kumar N, Joishi C, Xia Z, Rajan S and Kumar S 2019 Electrothermal simulation of delta-doped $\beta$-$Ga_2O_3$ field effect transistors *2019 18th IEEE Intersociety Conf. Thermal and Thermomechanical Phenomena in Electronic Systems (ITherm)*
[31] Blumenschein N A *et al* 2020 Self-heating characterization of $\beta$-$Ga_2O_3$ thin-channel MOSFETs by pulsed $I$–$V$ and Raman nanothermography *IEEE Trans. Electron Devices* **67** 204–11
[32] Santia M D, Tandon N and Albrecht J D 2015 Lattice thermal conductivity in $\beta$-$Ga_2O_3$ from first principles *Appl. Phys. Lett.* **107** 041907
[33] Loy J M 2013 An Efficient Solution Procedure for Simulating Phonon Transport in Multiscale Multimaterial Systems *PhD Dissertation* The University of Texas Austin
[34] Kresse G and Furthmüller J 1996 Efficiency of *ab initio* total energy calculations for metals and semiconductors using a plane-wave basis set *Comput. Mater. Sci.* **6** 15–50
[35] Kresse G and Furthmüller J 1996 Efficient iterative schemes for *ab initio* total-energy calculations using a plane-wave basis set *Phys. Rev.* B **54** 11169–86
[36] Blöchl P E 1994 Projector augmented-wave method *Phys. Rev.* B **50** 17953–79
[37] Kresse G and Joubert D 1999 From ultrasoft pseudopotentials to the projector augmented-wave method *Phys. Rev.* B **59** 1758–75
[38] Perdew J P, Burke K and Ernzerhof M 1996 Generalized gradient approximation made simple *Phys. Rev. Lett.* **77** 3865–8
[39] Togo A and Tanaka I 2015 First principles phonon calculations in materials science *Scr. Mater.* **108** 1–5
[40] Maradudin A A and Fein A E 1962 Scattering of neutrons by an anharmonic crystal *Phys. Rev.* **128** 2589–608
[41] Li W, Carrete J, Katcho N A and Mingo N 2014 ShengBTE: a solver of the Boltzmann transport equation for phonons *Comput. Phys. Commun.* **185** 1747–58
[42] Li W, Mingo N, Lindsay L, Broido D A, Stewart D A and Katcho N A 2012 Thermal conductivity of diamond nanowires from first principles *Phys. Rev.* B **85** 195436
[43] Li W, Lindsay L, Broido D A, Stewart D A and Mingo N 2012 Thermal conductivity of bulk and nanowire $Mg_2Si_xSn_{1-x}$ alloys from first principles *Phys. Rev.* B **86** 174307
[44] Ni C 2009 Phonon transport models for heat conduction in submicron geometries with application to microelectronics *PhD Dissertation* Purdue University, Ann Arbor p 176
[45] Mengle K A and Kioupakis E 2019 Vibrational and electron–phonon coupling properties of $\beta$-$Ga_2O_3$ from first-principles calculations: impact on the mobility and breakdown field *AIP Adv.* **9** 015313
[46] Cheng Z, Wheeler V D, Bai T, Shi J, Tadjer M J, Feygelson T, Hobart K D, Goorsky M S and Graham S 2020 Integration of polycrystalline $Ga_2O_3$ on diamond for thermal management *Appl. Phys. Lett.* **116** 062105
[47] Handwerg M, Mitdank R, Galazka Z and Fischer S F 2015 Temperature-dependent thermal conductivity in Mg-doped and undoped $\beta$-$Ga_2O_3$ bulk-crystals *Semicond. Sci. Technol.* **30** 024006